Analysis note for:

Fluctuations of charge separation perpendicular to the reaction plane and possible local parity violation in Au+Au collisions at $\sqrt{s_{NN}}$ = 7.7 - 62.4 GeV

Contact person: Gang Wang (UCLA) gwang@physics.ucla.edu

Fluctuations of charge separation perpendicular to the reaction plane and local parity violation in Au+Au collisions at $\sqrt{s_{NN}}$ = 7.7 - 62.4 GeV

1．Introduction

The main goal of this analysis is to study the beam energy dependency of the three-point correlator, used to reveal the charge separation perpendicular to the reaction plane. One interesting mechanism to induce such charge separation is via the local parity violation in the strong interaction and the chiral magnetic effect. In RHIC run10 and run11, Au+Au collisions at different beam energies were carried out. When the center-of-mass energy is 7.7 GeV, presumably QGP is turned off and so is the related chiral magnetic effect. In that case, we would expect a falling of the charge-separation signal towards 7.7 GeV.

2．Analysis

This analysis closely follows the three previous STAR papers on the same topic, with the three-point correlator γ defined in the following way:

$$\gamma \equiv \left\langle \cos(\varphi_1 + \varphi_2 - 2\psi_{RP}) \right\rangle \tag{1}$$

where φ and ψ denote the azimuthal angles of a particle and the reaction plane, respectively. The two particles each could be positively or negatively charged, and we use γ_{OC} and γ_{SC} to represent the opposite charge and the same charge correlation, respectively.

2.1 Analysis Code

The analysis code is located: /$CVSROOT/offline/paper/psn0595. We carried out the analysis in two steps: first the standard STAR "StFlowMaker" and "StFlowAnalysisMaker" were modified to generate Tree-structure ROOT files; then the macro "Parity.C" was used to calculate the correlator. The centrality was determined with the official centrality definition, "MyRef.h", a modified version of "StRefMultCorr". The re-weighting factors were also applied according to the above Maker.

2.2 Event Selection

The files were cataloged with the conditions listed in Table 1.

$\sqrt{s_{NN}}$ (GeV)	Production	Trigger Setup	# events	Trigger ID
62.4	P04id, P04ie	production62GeV	8 M	35001 35004 35007 35007
39	P10ik	AuAu39_production	100M	280001
27	P11id	AuAu27_production_2011	46M	360001
19.6	P11id	AuAu19_production	20M	340001 340011 340021
11.5	P10ih	AuAu11_production	10M	310004 310014
7.7	P10ih	AuAu7_production	4M	290001

Table 1: Conditions to select MuDst files.

A minimum bias trigger was used with events sorted into centrality classes based on charged particle multiplicity. The trigger IDs are listed in Table 1. The vertex Z cut is within 30cm for 62.4 GeV, 40 cm for 39, 27 and 19 GeV, 50 cm for 11.5 GeV and 70 cm for 7.7 GeV. For 39 GeV, we also required |TPC Vz - VPD Vz| < 4 cm and BBC coincident rate < 10000 to suppress the pile-up events due to the high luminosity. This cut will be discussed in Sec 3.5. To suppress events from collisions with the beam pipe (radius 3.95 cm), a cut on the radial position of the reconstructed primary vertex within 2 cm was applied for all the beam energies.

2.3 Track Selection

Charged particle tracks in this analysis were reconstructed in the STAR Time Projection Chamber (TPC) , with a pseudo-rapidity cut $|\eta| < 1$ and a transverse momentum cut $0.15 < p_T < 2$ GeV/c. The following track quality cuts were applied: the number of total hit points was larger than 20, and the ratio of the number of reconstructed hits to the maximum possible number of hits for each track was larger than 0.52. A cut on the distance of the closest approach to the primary vertex (DCA < 2 cm) was

also applied to reduce the number of weak decay tracks or secondary interactions. The two charged particles involved in the analysis have been corrected for the tracking efficiency, which will be discussed in Sec 2.5.

2.4 Event Plane

The reaction plane of a heavy-ion collision is not known a priori, and in practice it is approximated with the event plane reconstructed from particle azimuthal distributions. In this analysis, we exploited the large elliptic flow of charged hadrons produced at mid-rapidity:

$$\psi_{EP} = \frac{1}{2}\tan^{-1}\left[\frac{\sum \omega_i \sin(2\varphi_i)}{\sum \omega_i \cos(2\varphi_i)}\right],$$ (2)

where ω_i is a weight for each particle i in the sum. The weight was chosen to be the p_T of the particle itself. Although the STAR TPC has good azimuthal symmetry, small acceptance effects in the calculation of the event plane azimuth were removed by the method of shifting. The observed correlations were corrected for the event plane resolution, which was estimated with the correlation between two random sub-events.
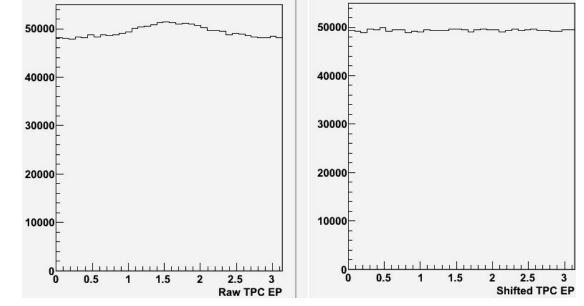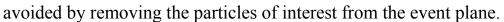

Figure 1: Example of the shifting method for 50-60% Au+Au at 39 GeV.

The effect of the shifting method is demonstrated in Fig. 1. The same procedure was also applied to the single particle azimuthal angle to further remove the artificial correlations due to the acceptance defects. The shifting procedure was carried out separately for each time interval. Figure 2 shows the event plane resolution as a function of centrality for all the beam energies under study. Self-correlations in the analysis were
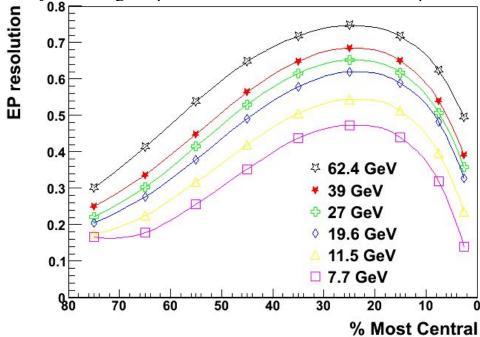
avoided by removing the particles of interest from the event plane.

Figure 2: The event plane resolution as a function of centrality.

2.5 Efficiency

The tracking efficiency is roughly a constant over pseudo-rapidity as shown in Fig 3, but not a constant over p_T, and varies with the occupancy and the detector performance. Figure 4 shows the pion tracking efficiency as a function of p_T for 70-80% Au+Au collisions from 200 GeV (run7) to 7.7 GeV, determined from embedding data. The efficiency for 62.4 GeV Au+Au (run4) was interpolated from the known efficiency for 200 GeV (run4). The tracking efficiency for run4 200 GeV was obtained from embedding data by previous STAR collaborators for PID analyses. Assuming for the same year the detector condition and the tracking algorithm are not significantly changed, the tracking efficiency will be a function of occupancy. Thus we can interpolate the efficiency according to the multiplicity from 200 GeV to 62.4 GeV.

The inverse of the tracking efficiency was used as a weight for each particle in the correlation. The correction restores the low p_T contribution to the correlations. The systematic uncertainties on the LPV correlations due to the tracking efficiency are estimated to be below relative 5%. (More discussion in Sec 3.5.)
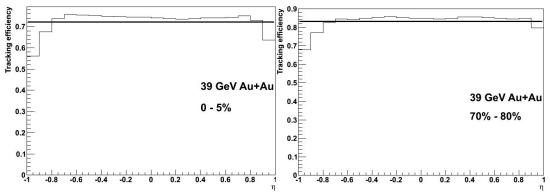
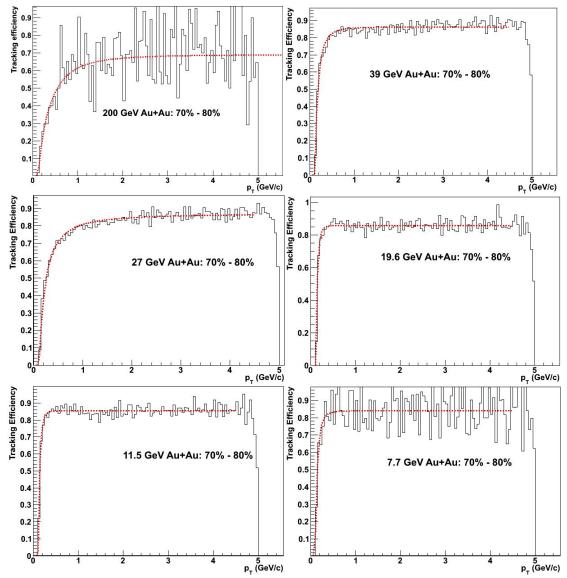**Figure 3: The tracking efficiency vs η for 0-5% and 70-80% Au+Au collisions.**

Figure 4: The tracking efficiency as a function of p_T for 70-80% Au+Au collisions from 200 GeV to 7.7 GeV.

3. Results

3.1 62.4 GeV

The published run4 results of 62.4 GeV data only used 2.8M events. In this analysis, we used the full statistics of 7M events from run4, and the results are consistent with the published data with smaller statistical errors as shown in Fig. 5 (both uncorrected for the tracking efficiency).
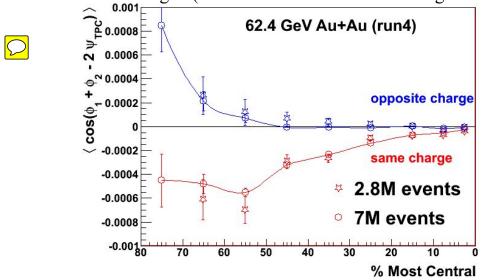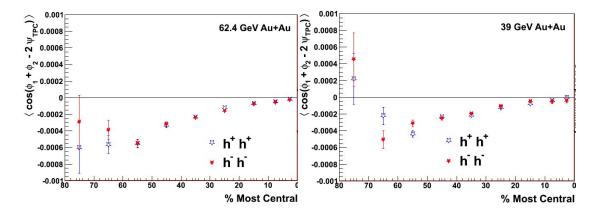

Figure 5: The comparison between old and new correlation results for 62.4 GeV Au+Au collisions

3.2 ++ and --

As a systematic check, we compared γ_{++} and γ_{--} and found reasonable consistency between them for all the centrality bins at all energies.
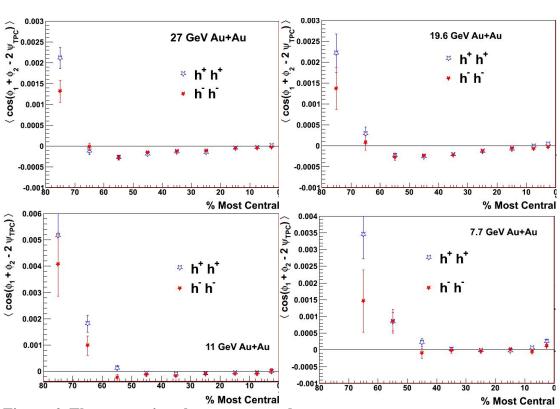
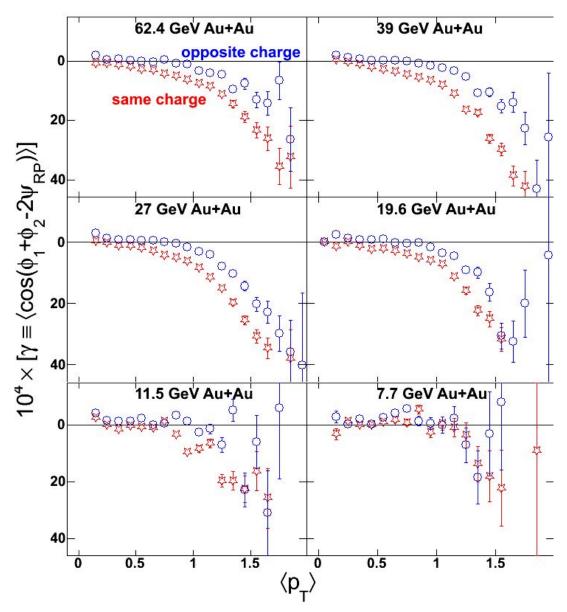**Figure 6: The comparison between γ++ and γ---.**

3.3 Differential measurements

Figure 7: γ_{OS} and γ_{SS} as a function of $<p_T> = (p_{T1}+p_{T2})/2$ for 30-60% Au+Au collisions at $\sqrt{s_{NN}} = 7.7 - 62.4$ GeV.

Figure 7-10 shows the differential measurements of the three-point correlator for 30-60% Au+Au collisions for all the beam energies under study. The difference between opposite charge and same charge increases with $<p_T>$ in most cases, except at 7.7 GeV, where the difference almost disappears. Figure 8 shows that the signal is stronger in mid-rapidity, which is understandable since that is where QGP is most likely to occur.
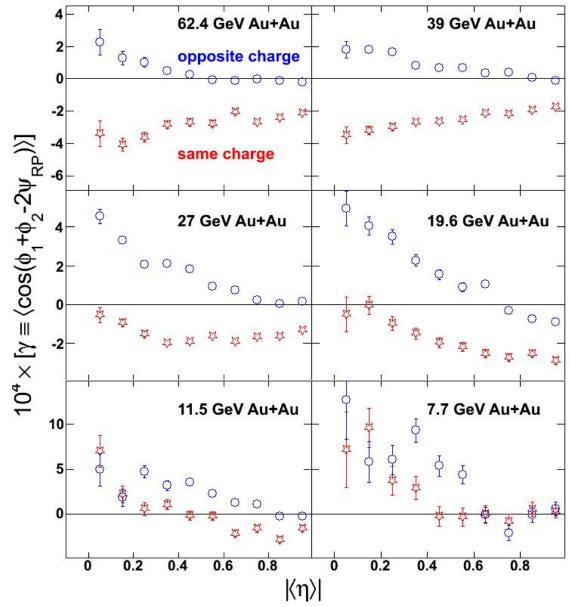
Figure 8: γ_{OS} and γ_{SS} as a function of $|<\eta>| = |(\eta_1+\eta_2)/2|$ for 30-60% Au+Au collisions at $\sqrt{s_{NN}} = 7.7 - 62.4$ GeV.

The correlations vs Δp_T and $\Delta\eta$ in Fig. 9 and 10 also show that the signal almost disappears at 7.7 GeV. The finite difference between opposite charge and same charge at 7.7 GeV is mostly found in low relative p_T and η and these are the so-called femtoscopic correlation region. The study of such effects will be discussed in the next section.
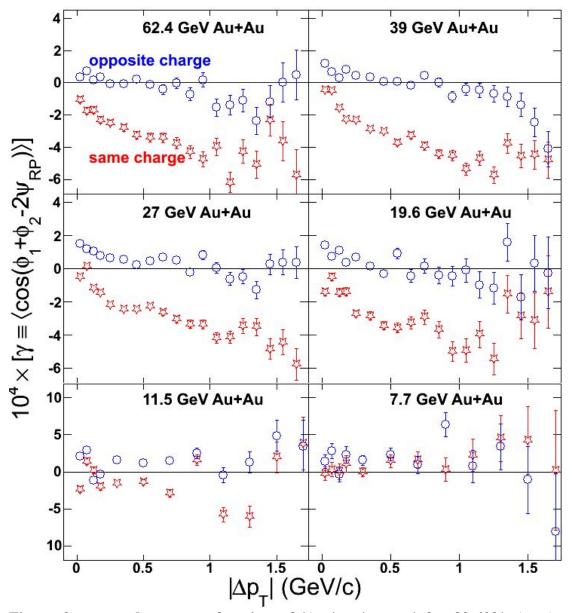
Figure 9: γ_{OS} and γ_{SS} as a function of $|\Delta p_T| = |p_{T1}-p_{T2}|$ for 30-60% Au+Au collisions at $\sqrt{s_{NN}} = 7.7 - 62.4$ GeV.
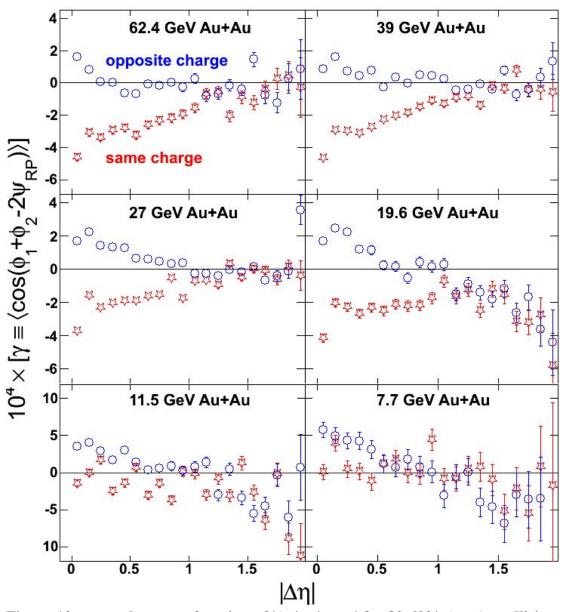
Figure 10: γ_{OS} and γ_{SS} as a function of $|\Delta\eta| = |\eta_1 - \eta_2|$ for 30-60% Au+Au collisions at $\sqrt{s_{NN}} = 7.7 - 62.4$ GeV.

3.4 HBT and Coulomb Effects

Figures 11 and 12 take $30 - 60\%$ Au+Au collisions at 200 and 39 GeV as an example, to show the composite parts of the three-point correlator differentially versus (a) $|\Delta p_T|$ and (b) $|\Delta\eta|$. The subtraction of out-of-plane ($<\sin(\Delta\varphi_1)\sin(\Delta\varphi_2)>$) from in-plane ($<\cos(\Delta\varphi_1)\cos(\Delta\varphi_2)>$) composite parts yields the original γ, while the sum yields a two particle correlation, $<\cos(\varphi_1 - \varphi_2)>$. The split correlations reveal the underlying P-even background affecting both composite parts as each part is sensitive to correlations independent of the reaction plane. For both γ_{OS} and γ_{SS}, the functional shape of in-plane and out-of-plane parts are similar.

13

The magnitudes of in-plane and out-of-plane parts are more different for same charge pairs.
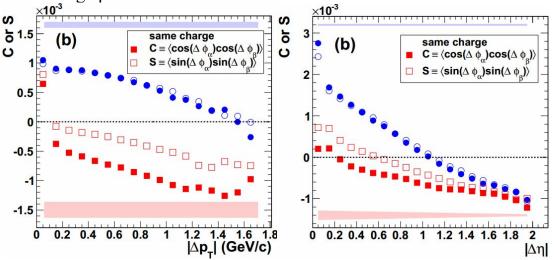

Figure 11: γ split up into in-plane and out-of-plane composite parts for 30−60% Au+Au collisions at 200 GeV. (a) shows the correlations versus $|\Delta p_T| = |p_{T,1} - p_{T,2}|$. (b) shows the correlations versus $|\Delta \eta| = |\eta_1 - \eta_2|$.

Figure 12: γ split up into in-plane and out-of-plane composite parts for 30−60% Au+Au collisions at 39 GeV. (a) shows the correlations versus $|\Delta p_T| = |p_{T,1} - p_{T,2}|$. (b) shows the correlations versus $|\Delta \eta| = |\eta_1 - \eta_2|$.
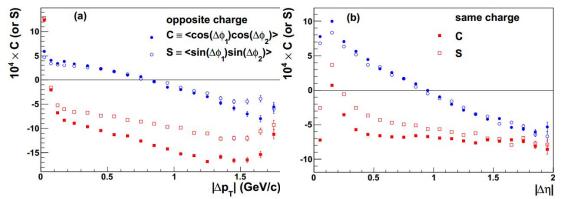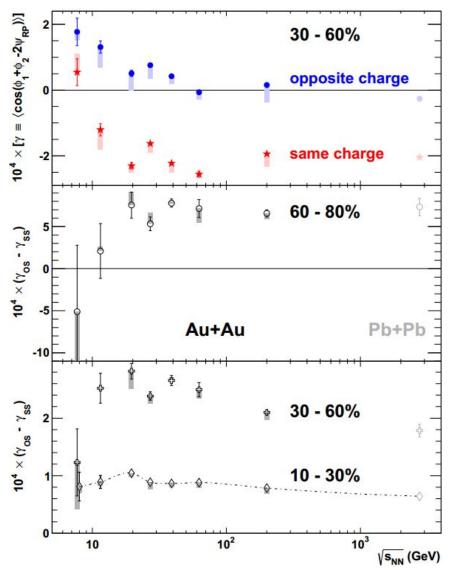
Figure 13: γ_{OS} and γ_{SS} as a function of beam energy for 30−60% Au+Au collisions (upper), and (γ_{OS}-γ_{SS}) for different centralities (middle and lower). For comparison, the results for Pb+Pb collisions at 2.76 TeV are also shown. The systematic errors of the STAR data (filled boxes) are obtained with the conditions of $\Delta p_T > 0.15$ GeV/c and $\Delta\eta > 0.15$ to suppress HBT+Coulomb effects.

In the lowest bins in Fig. 11 and 12, shape changes are visible for same charge pairs in panel (a) and for both opposite and same charge pairs in panel (b). Such changes can be attributed to quantum interference ("HBT" effects) and final-state-interactions (Coulomb dominated), which are most prominent for low relative momentum. To suppress the contributions from these effects, we applied the conditions of $\Delta p_T > 0.15$ GeV/c and $\Delta\eta > 0.15$ to the three-point correlator in the paper. Figure 13 shows that with these conditions, $\gamma_{OS} - \gamma_{SS}$ remains largely unchanged for most energies, and at 7.7 GeV the already small difference roughly reduces by half. The above conditions are shown with the filled boxes in Fig 14 for each centrality and each beam energy under study.
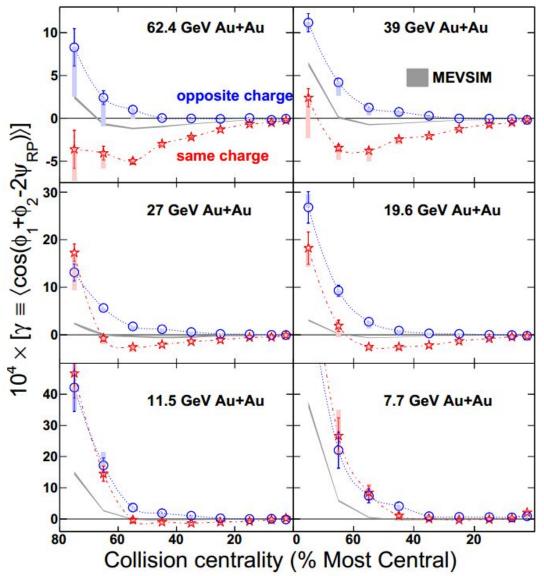
Figure 14: γ_{OS} and γ_{SS} as a function of centrality for Au+Au collisions at $\sqrt{s_{NN}}$ = 7.7 - 62.4 GeV. Charge-independent MEVSIM calculations are also shown.

3.5 More Systematics

The systematic uncertainty due to the event plane determination was studied with run7 data for 200 GeV Au+Au, as shown in Fig. 15. (γ_{OS}-γ_{SS}), on average, is consistent between EP{TPC} and EP{ZDC} within the statistical errors. At lower beam energies, the ZDC efficiency becomes too low to be used for the event plane, and we assign a relative 10% systematic uncertainty to this source.
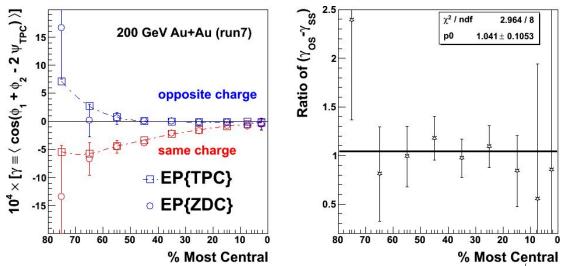
Figure 15: γ_{OS} and γ_{SS} as a function of centrality for Au+Au collisions at $\sqrt{s_{NN}} =$ 200 GeV (run7) with the event plane reconstructed from TPC and ZDC. The ratios of (γ_{OS}-γ_{SS}) from the two methods are shown in the right panel.
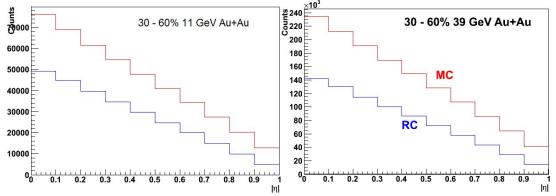

Figure 16: The distributions of $|\langle\eta\rangle| = |(\eta_1+\eta_2)/2|$ for Monte Carlo track pairs and reconstructed track pairs for 30-60% Au+Au collisions at 11 and 39 GeV.

The η dependence of the tracking efficiency is not flat, and the effect can be studied via the mean η of the track pairs. Fig. 16 shows such distributions for Monte Carlo tracks and reconstructed paris for 30-60% Au+Au collisions at 11 and 39 GeV. When (γ_{OS}-γ_{SS}) in Fig 8 is integrated over $|\langle\eta\rangle|$ with the weights from Fig 16, the difference is on a relative 2~3% level for all the beam energies under study. Together with the efficiency uncertainty in the p_T dependence, we quote a relative 5% systematic error from this source.

We also varied the vertex Z cut to study the corresponding systematics. For 62.4 GeV, the cut was reduced from 30 to 20 cm, and for 30-60% centrality range the change in (γ_{OS}-γ_{SS}) is relative 0.05%. For 39 GeV, the cut was reduced from 40 to 30 cm, and for 50-60% centrality range the change in (γ_{OS}-γ_{SS}) is relative 1.9%. For 27 GeV, the cut was reduced from 40 to 30 cm, and for 30-60% Au+Au the relative change is 5.4%. For 19 GeV, the cut was reduced from 40 to 30 cm, and for 30-60%

centrality range the relative change is 3.7%. For 11.5 GeV, the cut was reduced from 50 to 40 cm, and for 30-60% centrality range the change is relative 4.8%. For 7.7 GeV, the cut was reduced from 70 to 60cm, and the relative change for 30-60% centrality range is 30.2%, but (γ_{OS}-γ_{SS}) is close to zero and the statistical errors are relatively large.

We also reduced the DCA cut from 2cm to 1 cm to study the corresponding systematics. For 30-60% Au+Au at 62.4 GeV, the change in (γ_{OS}-γ_{SS}) is relative 6.6%. For 50-60% Au+Au at 39 GeV, the relative change is 7.2%. For 30-60% Au+Au at 27 GeV, the relative change is 2.6%. For 50-60% Au+Au at 19 GeV, the relative change is 0.97%. For 30-60% Au+Au at 11.5 GeV, the change is relative 10%. For 30-60% Au+Au at 7.7 GeV, the change is relative 31.2%, but (γ_{OS}-γ_{SS}) is close to zero and the statistical errors are relatively large.

We also studied the effect of the BBC coincident rate. For other energies than 39 GeV, the BBC rate is always lower than 10000, and we don't worry much about the luminosity effect. For 39 GeV, when we applied the condition of BBC rate <10000, the number of good events reduces from 100 to 23 million. For 60-80% collisions at 39 GeV, we used all the events including those with BBC rate > 10000, and the difference is relative 5.5%, smaller than the statistical errors.

In short, the systematic uncertainties due to the analysis cuts are estimated to be within relative 10%. Together with the errors due to the tracking efficiency (5%) and the event plane determination (10%), we conclude that the total systematic errors are typically within 15% for (γ_{OS}-γ_{SS}) when it's not close to zero.

3.6 Further interpretation

(γ_{OS}-γ_{SS}) may still contains flow contribution. We take the following assumption, trying to remove or suppress flow contribution:

$$\gamma \equiv \left\langle \cos(\varphi_1 + \varphi_2 - 2\psi_{RP}) \right\rangle = \kappa v_2 F - H \qquad (2)$$

$$\delta \equiv \left\langle \cos(\varphi_1 - \varphi_2) \right\rangle = F + H \qquad (3)$$

where F and H are flow and CME contributions, respectively. κ is typically between 1 and 2, quantifying the theoretical uncertainty. F includes physics mechanisms like Transverse Momentum Conservation (TMC), Local Charge Conservation (LCC), jets and so on. The TMC contribution was discussed in *Phys. Rev. C 83 (2011) 014905*:

$$\langle\cos(\phi_1+\phi_2)\rangle = -\frac{1}{N}\frac{\langle p_t\rangle_\Omega^2}{\langle p_t^2\rangle_F}\frac{2\bar{v}_{2,\Omega}-\bar{\bar{v}}_{2,F}-\bar{\bar{v}}_{2,F}(\bar{v}_{2,\Omega})^2}{1-(\bar{\bar{v}}_{2,F})^2} \tag{4}$$

$$\langle\cos(\phi_1-\phi_2)\rangle = -\frac{1}{N}\frac{\langle p_t\rangle_\Omega^2}{\langle p_t^2\rangle_F}\frac{1+(\bar{v}_{2,\Omega})^2-2\bar{\bar{v}}_{2,F}\,\bar{v}_{2,\Omega}}{1-(\bar{\bar{v}}_{2,F})^2} \tag{5}$$

With the first order approximation, we have the proportionality between the TMC contributions in γ and δ to be $\kappa v_2 = 2v_2 - v_{2,F}$, where v_2 is the measured elliptic flow within the detector acceptance and $v_{2,F}$ is the elliptic flow in the full phase space. According to the estimation of the paper above for the STAR acceptance, κ is roughly 1.13, pretty close to unity. For other effects lie LLC and jet in F, Ron Longacre argued in the preprint arXiv:1112.2139 that the proportionality still holds.

With γ and δ measured in this analysis, and v2 from previous publications, we can solve for H:

$$H^\kappa = (\kappa v_2 \delta - \gamma)/(1+\kappa v_2) \tag{6}$$

Note that H has an opposite sign to γ. Figure 17 shows δ as a function of centrality for each beam energy under study. δ_{OS} is in most cases higher than δ_{SS}, indicating the non-zero F. Figure 18 shows H_{SS} and H_{OS} as a function of centrality for each beam energy under study, with κ set to be unity .
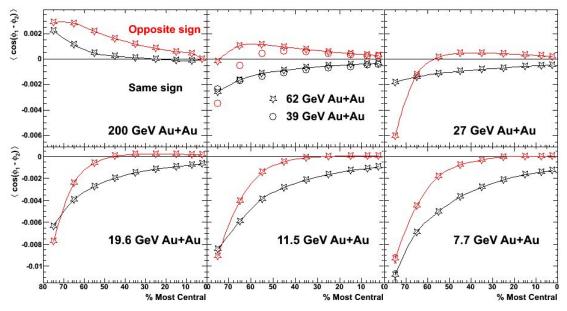

Figure 17: δ as a function of centrality for all the energies under study.

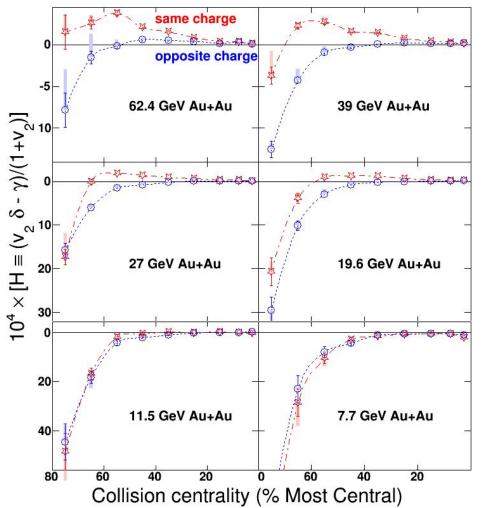**Figure 18: H_{SS} and H_{OS} as a function of centrality for all the energies under study.**

Now at high energies, H_{SS} is above H_{OS} as expected by LPV+CME. At lower energies ~ 7.7 GeV, the signal (H_{SS} - H_{OS}) seems to disappear. Some charge-independent background is still present in H. The data points in Fig. 18 are combined and rearranged in Fig. 19 to better display the beam energy dependency of the signal. The systematic uncertainty bands for 30-60% centrality range is obtained with κ=1.5.
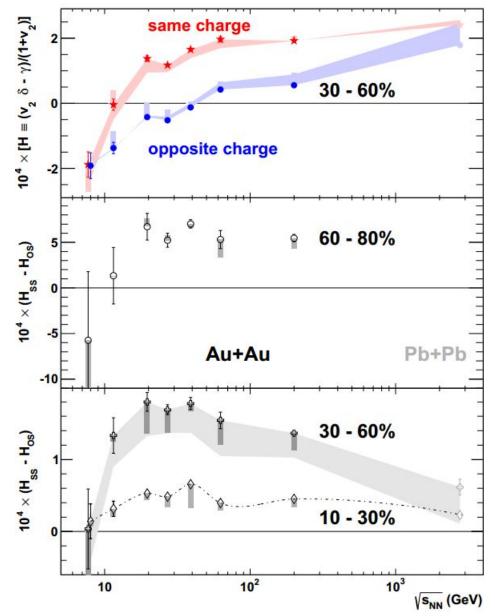
Figure 19: H_{SS} and H_{OS} separately as a function of beam energy for 30-60% Au+Au collisions (upper), and (H_{SS} - H_{OS}) for different centralities (middle and lower).

4. Simulation (MEVSIM)

The MEVSIM code was developed to provide a quick means of producing uncorrelated simulated events for event-by-event studies, detector acceptance and efficiency studies, etc. The user selects the number of events, the one-particle distribution model, the particles to include, the ranges in transverse momentum, pseudo-rapidity and azimuthal angle, the mean multiplicity for each particle type for the event run, the mean temperature, Rapidity width, etc., and the standard deviations for the event-to-event variation in the model parameters.

We used an updated version of MEVSIM which implements momentum conservation. Each event was produced according to the charged multiplicity for a specific centrality at a specific beam energy. v_2 was imposed to each particle according to previous v_2 measurements. Then the simulation events were analyzed in the same way as the real data. The charge-independent correlations from MEVSIM are shown in filled boxes in Fig 13, and qualitatively describe the beam-energy dependency of the charge-independent background of the three-point correlator.